



X-ray Cross-Correlation Analysis of Mesocrystals

Dmitry Lapkin

Moscow Institute of Physics and Technology, Moscow, Russia

Supervisors: Nastasia Mukharamova, Ivan Vartanians

DESY, Hamburg, Germany

Abstract

X-ray Cross-Correlation Analysis (XCCA) was employed to evaluate the crystalline structure of mesocrystals consisting of the lead sulfide nanocrystals linked with oleic acid. The superlattice was shown to have a body-centered tetragonal structure, either by means of XCCA analysis and by the XCCA simulations of the anticipated structure.

Contents

1. Introduction	2
2. Methods	3
2.1. X-ray diffraction	3
2.2. X-ray Cross-Correlation Analysis	5
2.3. Cross-Correlation Function Simulation.....	6
3. Results and discussion.....	7
3.1. Radial average	7
3.2. Spatially-resolved diffraction maps.....	7
3.3. X-ray Cross-Correlation Analysis	12
3.4. Superlattice structure evaluation	13
4. Conclusion.....	18
References	19

1. Introduction

Mesocrystals (MC) are three-dimensional arrays of iso-oriented single-crystalline particles with an individual size between 1 and 1000 nm [1]. Their physical properties are largely determined by structural coherence, for which the angular correlation between their individual atomic lattices and the underlying superlattice of nanocrystals (NC) is a key ingredient. Colloidal NCs stabilized by organic surfactants have been shown to be excellent building blocks for synthetic MCs with tailored structural properties. These are obtained by self-assembly of NCs from solution on a solid or liquid substrate by exploiting ligand–ligand interactions as reported in [2, 3]. Typically, ligands consist of wide-gap, bulky hydrocarbons which render the MCs insulating. In this work the MCs were synthesized using lead sulfide (PbS) NCs (shown in Fig. 1a) stabilized by oleic acid molecules (shown in Fig. 1b), forming a superlattice similar to the one shown in Fig. 2.

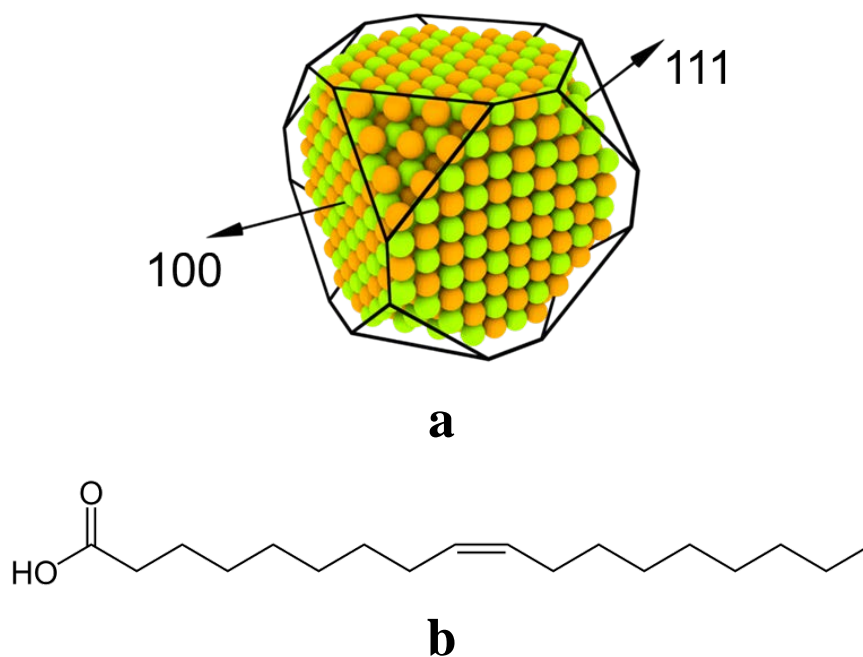


Figure 1. Main building blocks of the studied MC: a) schematic representation of a PbS nanocrystal (crystalline planes are indicated) and b) structure formula of the intercrystalline linker – oleic acid

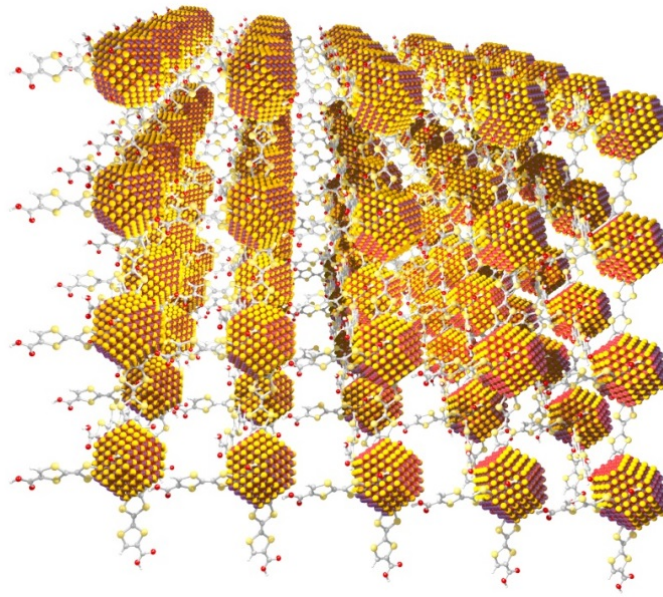


Figure 2. Structure of the superlattice consisting of PbS NCs (MC). NCs are linked with organic ligands

For X-ray experiments, the MCs were grown on a $500\ \mu\text{m} \times 500\ \mu\text{m}$ X-ray transparent window consisting of a 50 nm thick Si_3N_4 membrane (PLANO).

2. Methods

2.1. X-ray diffraction

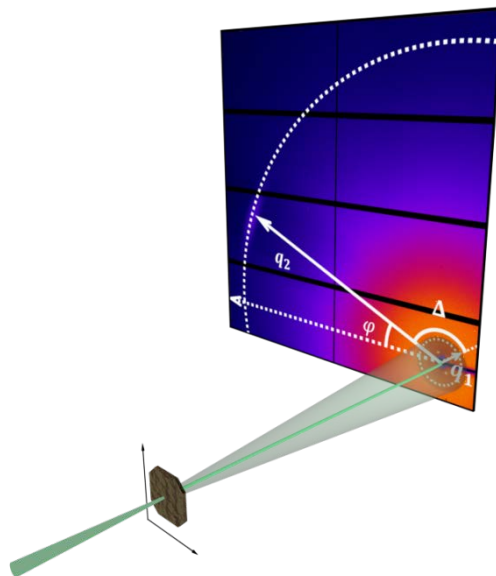


Figure 3. Schematic of the diffraction experiment. Incident beam was perpendicular to the sample surface. Detector was placed 41 cm from the sample. This geometry allows registering both SAXS and WAXS reflections.

The X-ray diffraction experiment was performed at the Coherence Beamline P10 of the PETRA III synchrotron source at DESY. The nanodiffraction endstation GINIX [4] was used to focus an X-ray beam with energy $E = 13.8$ keV ($\lambda = 0.898$ Å) down to 400×400 nm² size with KB-mirrors. The depth of the X-ray focus was about 0.5 mm. The sample was positioned perpendicular to the incoming X-ray beam as shown in Fig. 3. An area of 30×30 μm² was scanned to analyze the spatial variations of the samples' structure. Within this scanning region, 961 diffraction patterns were collected on the 31×31 raster grid with a ~ 1 μm step size in both directions perpendicular to the incident beam. Each diffraction pattern was collected with an exposure time of 0.5 s to prevent radiation damage, which was assessed by repeating the scanning procedure several times on the same position of the sample. A two-dimensional detector (2070x2167 pixels with 75×75 μm² size) was positioned downstream at a distance of 41 cm from the sample and shifted so to have transmitted beam close to a corner (as shown in Fig. 4). With this geometry, we were able to detect the scattering signal from the MC SL as well as from PbS AL simultaneously and only a part of reciprocal space in wide angle scattering was accessible. Then, the measured signal was corrected for background scattering. An example of the measured diffraction patterns is shown in Fig. 5, where both WAXS and SAXS (in inset) regions are visible.

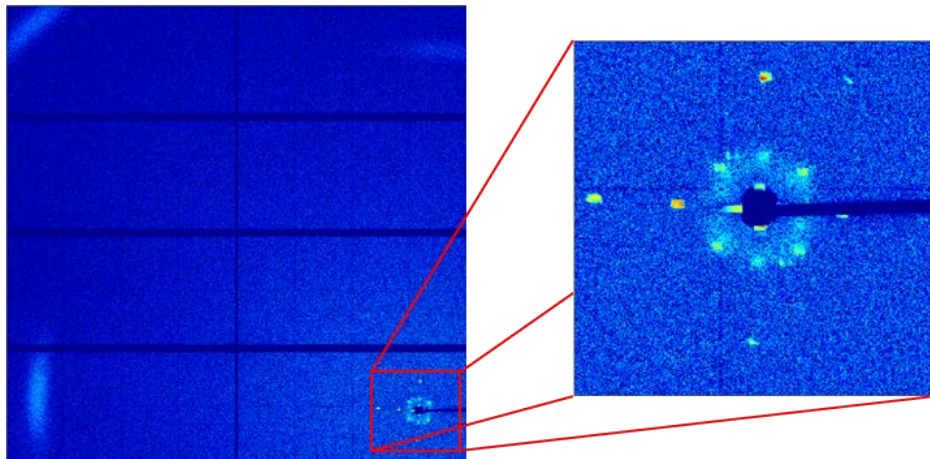


Figure 4. Example of the measured diffraction patterns of the MC. Both WAXS and SAXS (in inset) reflections are clearly visible. Dark areas are detector gaps, a beamstop etc.

2.2. X-ray Cross-Correlation Analysis

The XCCA method is widely used for the analysis of disordered or partially ordered systems such as colloids, liquid crystals, polymers etc. It provides information on angular correlations in the structure of molecules in the sample and on hidden symmetries and partial order of the system being studied. This method was also shown to be useful in the study of mesocrystals [6].

While details and mathematical background on this method could be found e.g. in [5], main ideas are as follows. A two-point angular cross-correlation function (CCF) that can be calculated for each diffraction profile as

$$C(q_1, q_2, \Delta) = \frac{1}{2\pi} \int_{-\pi}^{\pi} I(q_1, \varphi) I(q_2, \varphi + \Delta) d\varphi \quad (1)$$

where $I(q, \varphi)$ is the intensity of diffraction pattern at the point with distance from the center of the pattern q and angular position φ . All the values used in this definition are shown in Fig. 5.

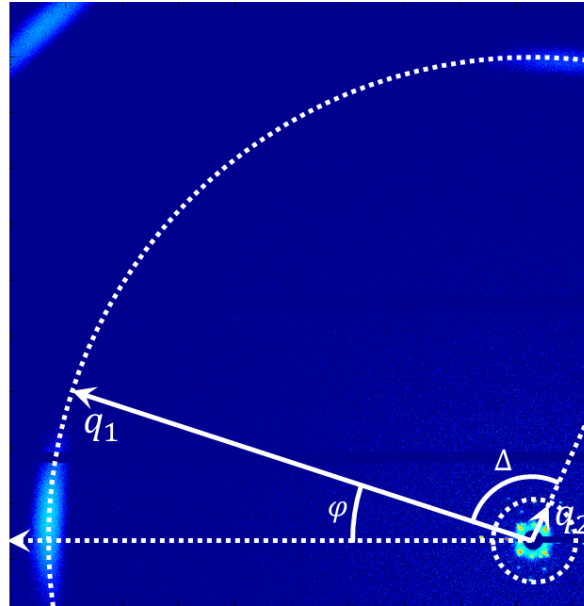


Figure 5. Graphical representation of variables used in the CCF definition. Arrows indicate the points of the diffraction patterns, in which the intensities are taken.

Experimentally obtained diffraction patterns contain defects such as detector gaps, beamstop, beamstop holder etc. In order to take into account their presence, we introduce into Eq. (1) the mask function

$$W(q, \varphi) = \begin{cases} 0, & \text{gaps, beamstop, detector edges} \\ 1, & \text{otherwise} \end{cases} \quad (2)$$

This gives us the final form of the CCF as in Eq. (3).

$$C(q_1, q_2, \Delta) = \frac{\int_{-\pi}^{\pi} I(q_1, \varphi) W(q_1, \varphi) I(q_2, \varphi + \Delta) W(q_2, \varphi + \Delta) d\varphi}{\int_{-\pi}^{\pi} W(q_1, \varphi) W(q_2, \varphi + \Delta) d\varphi} \quad (3)$$

Taking appropriate values of q_1 and q_2 we studied correlations between reflections in the WAXS and SAXS regions as well as autocorrelations in both regions. To obtain statistically meaningful data, CCFs were averaged over diffraction patterns from different points in the appropriate domain of the sample.

2.3. Cross-Correlation Function Simulation

The CCF function could be simulated assuming that Bragg peaks in both WAXS and SAXS regions have Gaussian shapes in the angular direction, i.e.

$$\frac{I_{SAXS}}{WAXS}(\varphi) = \frac{A_{SAXS}}{WAXS} \cdot \sum_i \exp\left(-\frac{\left(\varphi - \varphi_{SAXS}^i\right)^2}{2\sigma_{SAXS}^2}\right) \quad (4)$$

where $\frac{A_{SAXS}}{WAXS}$ is the amplitude of the peaks in the SAXS/WAXS region, φ_{SAXS}^i and σ_{SAXS} are the angular position and the angular size of the i-th SAXS/WAXS peak, respectively.

While in the experiment we were able to measure simultaneously the signal in the SAXS region for all azimuthal angles, in the WAXS region we were restricted by the detector size and measured the scattering signal only in the angular range of approximately 90° azimuthally. To simulate the effect of finite detector size we used the following mask for the WAXS signal

$$W(\varphi) = \begin{cases} 1, & \varphi_1 < \varphi < \varphi_2 \\ 0, & \text{otherwise} \end{cases} \quad (5)$$

where φ_1 and φ_2 are boundary angle values of the WAXS region area fitting into the detector.

The simulated CCF was then obtained according to the following procedure

$$CCF_{sim}(\Delta) = \int_{-\pi}^{\pi} I_{SAXS}(\varphi) I_{WAXS}(\varphi + \Delta) W(\varphi + \Delta) d\varphi \quad (6)$$

3. Results and discussion

3.1. Radial average

To investigate which peaks are contained in the diffraction patterns, we radially integrate scattered intensities for several lengths of the scattering vector with respect to the center of the incident beam. Resulting radial averages calculated for two different points of the sample are shown in Fig. 6.

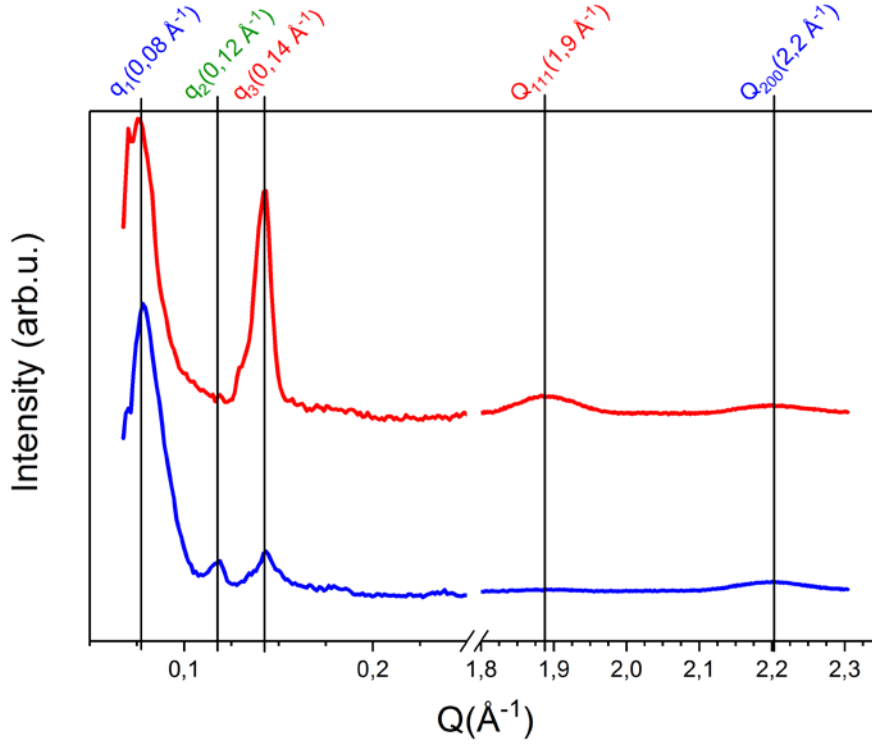


Figure 6. Radially averaged intensity of the diffraction patterns obtained from two points of the sample. To resolve SAXS region as well as WAXS one, a break was inserted.

We can resolve the two most intense peaks in the SAXS region with the momentum transfer values $q_1 = 0.08$ and $q_3 = 0.14 \text{ Å}^{-1}$ and attribute them to the scattering of the superlattice. The WAXS region contains peaks at 1.9 and 2.2 Å^{-1} , which from the literature correspond to $\{111\}$ and $\{200\}$ reflections of the PbS atomic lattice [7]. These values were used for finding the NC-containing area of the sample and later for obtaining spatially resolved maps of angular positions of the selected Bragg peaks in the diffraction patterns.

3.2. Spatially resolved diffraction maps

To find the NC-containing area of the sample, we evaluated the intensity of diffraction patterns in the WAXS region, corresponding to the scattering from the PbS atomic lattice. For

each diffraction pattern we integrated the intensity in the region with length of the scattering vector in the range $1.8 - 2.3 \text{ \AA}^{-1}$ (shown in Fig. 7a). This way we create a spatially resolved map of the intensity in the WAXS region, which is shown in Fig. 7b as a heat map. The red and yellow points contain the NCs, whereas there are no NCs in the blue points. One can distinguish several domains containing NCs separated by points with low intensity.

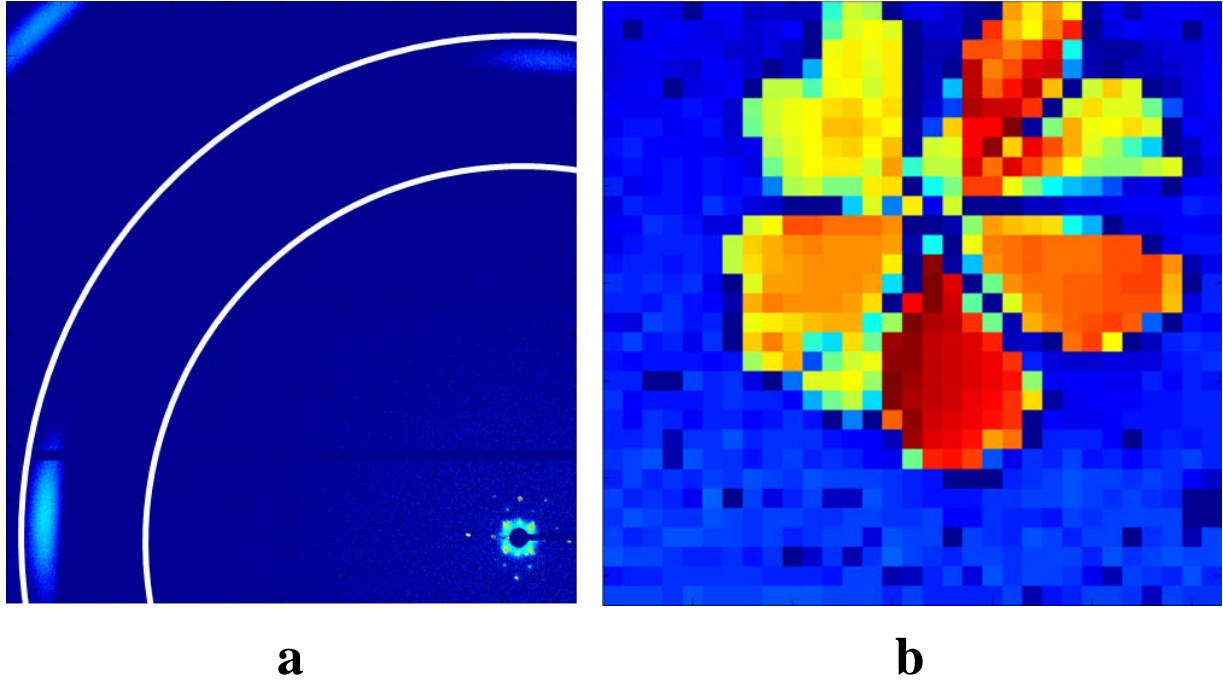
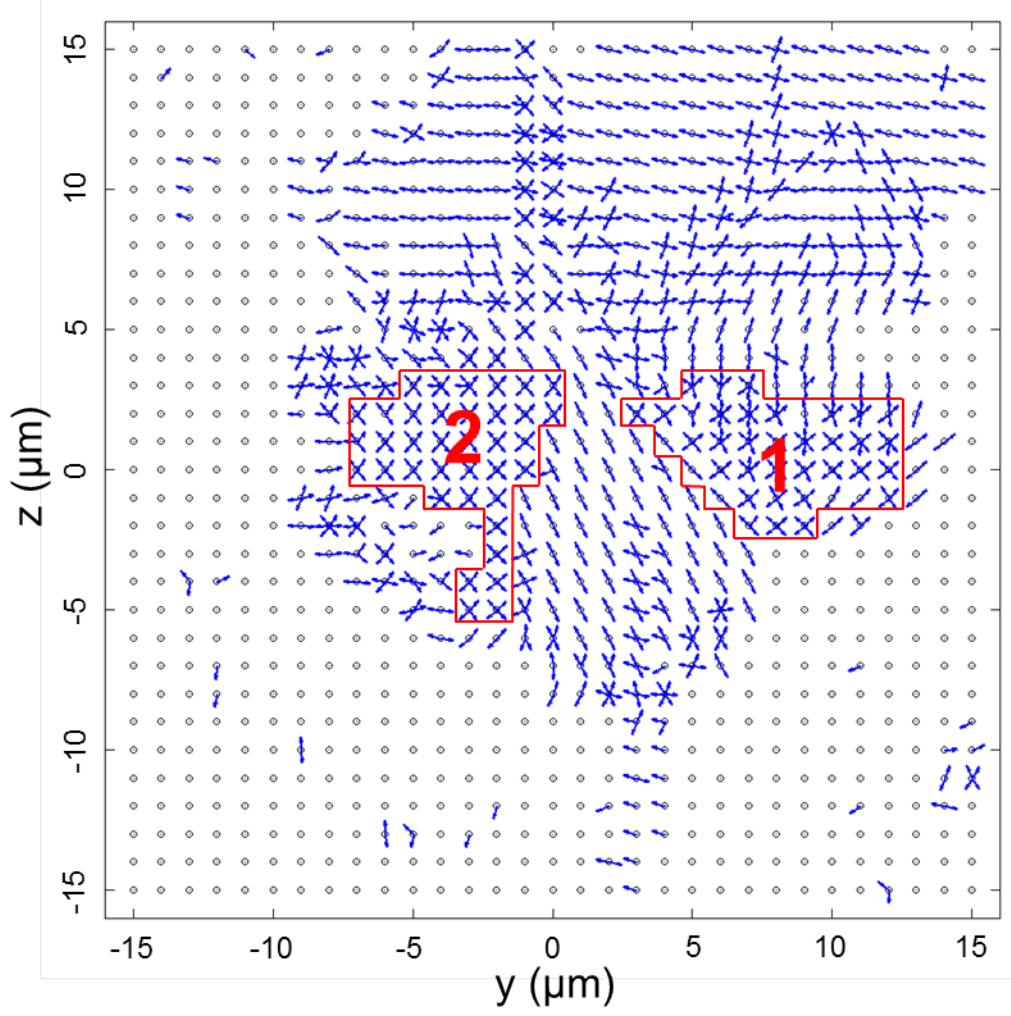
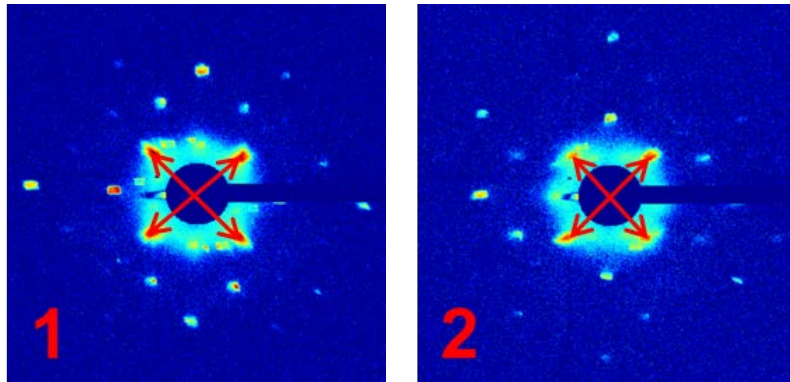


Figure 7. *a* – Region of a diffraction pattern used to calculate the intensity of diffraction in WAXS region; *b* – spatially resolved map of the intensity in the WAXS region

To study the crystalline structure of the domains we found the positions of each peak with a certain length of scattering vector in every point of the sample and marked these positions with arrows from the center of beam. The spatial-resolved map obtained for the length of the scattering vector of 0.08 \AA^{-1} (SAXS peaks) is shown in Fig. 8a. The visible domains with arrows are in a good agreement with the ones visible in Fig. 7b with some distortion on the edges. The two most promising domains are highlighted by red lines. Enlarged SAXS regions of the diffraction patterns averaged over these domains are shown in Fig. 8b. Since they contain more than one pair of diffraction peaks, they could provide us meaningful information about the crystalline structure (will be discussed below).



a



b

Figure 8. a – Spatially resolved map of the Bragg peaks positions relating to length q_l of the scattering vector in the SAXS region. Two domains are highlighted by red lines. b – Typical SAXS diffraction patterns obtained from the domains 1 and 2

In the same way we obtained a spatially-resolved map for the peaks with $q = 0,14 \text{ \AA}^{-1}$ (shown in Fig. 9a). From Fig. 9 we can conclude that there is only one domain, containing two pairs of the peaks. The enlarged SAXS region of the diffraction patterns of this domain is shown in Fig. 9b.

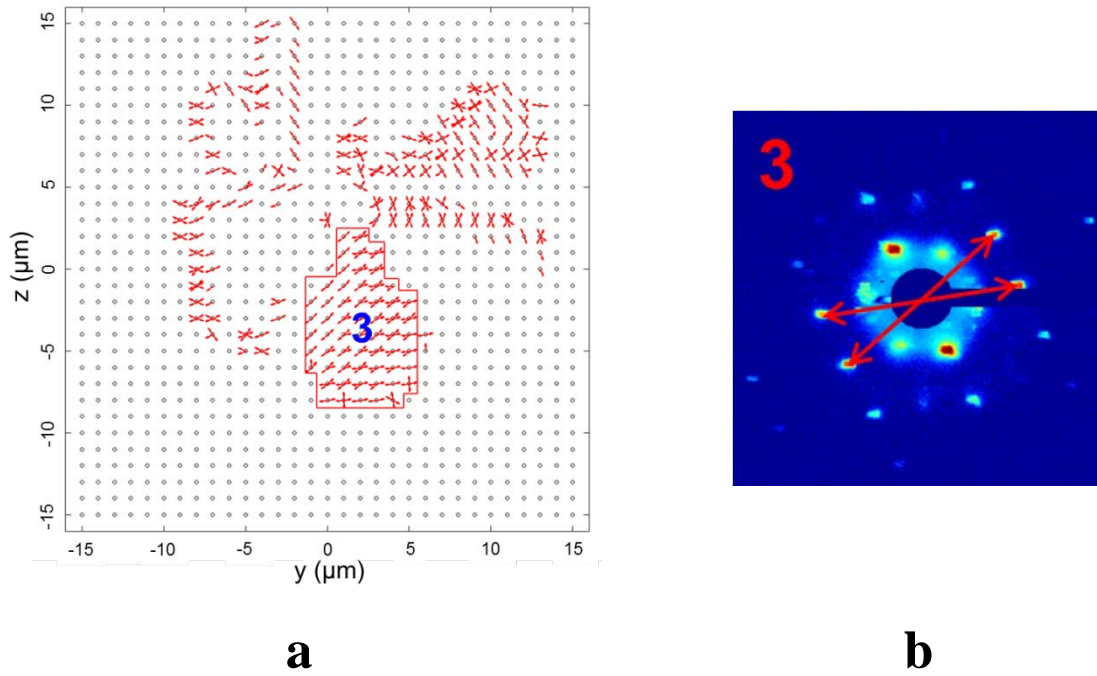
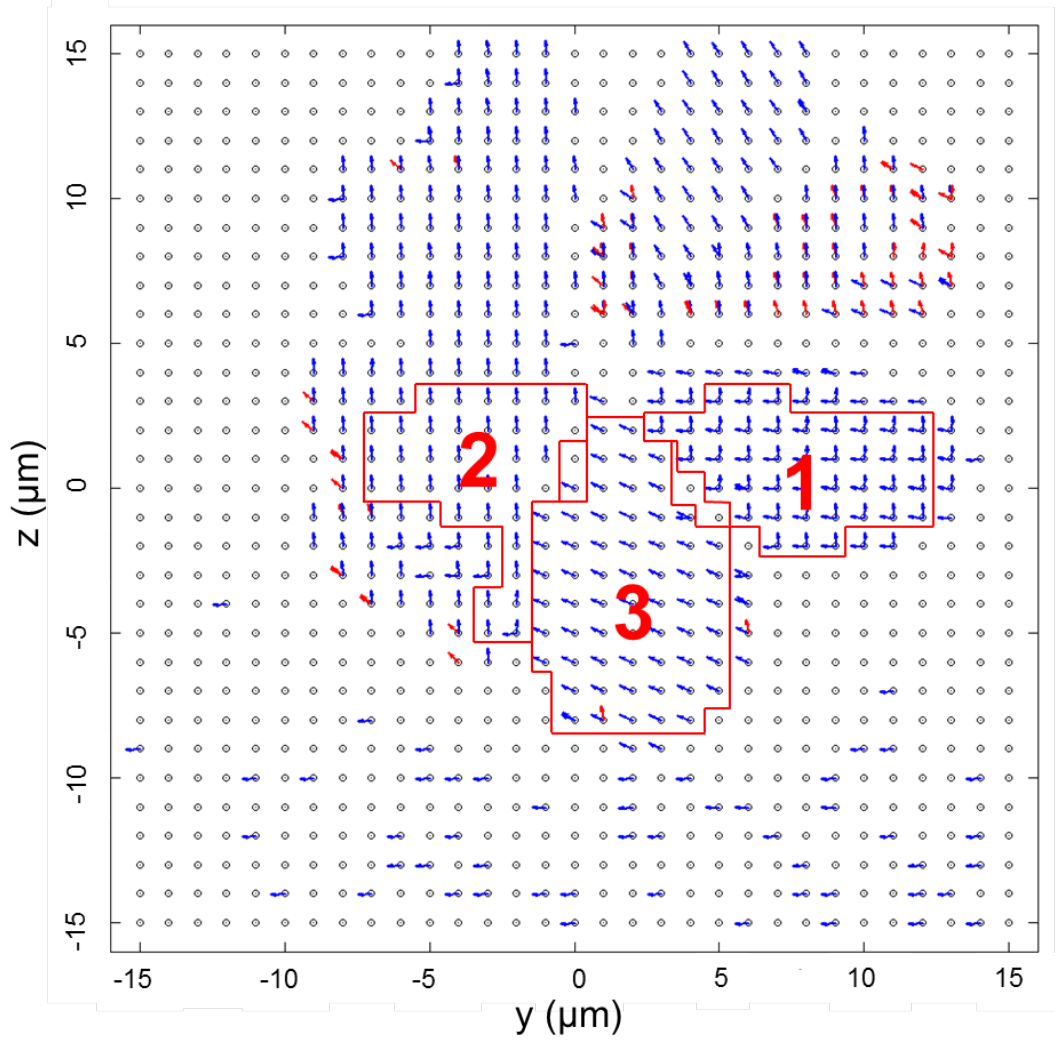
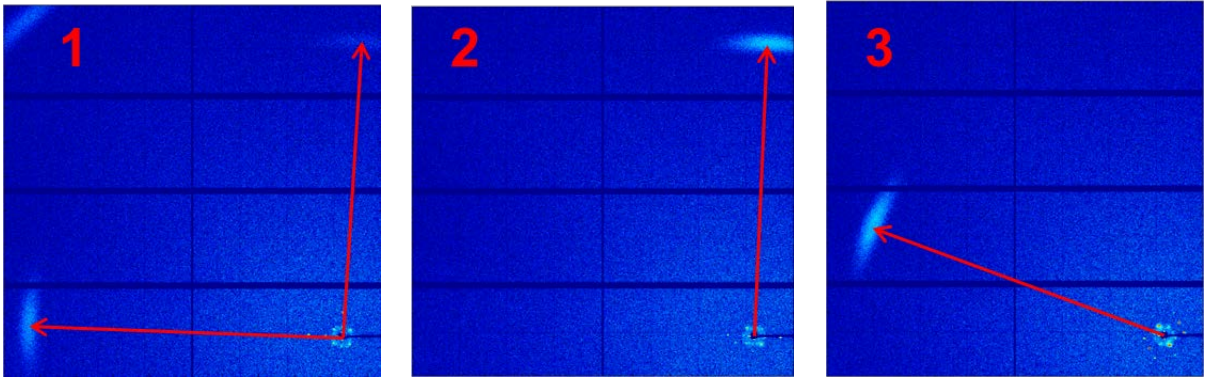


Figure 9. a – Spatially resolved map of the Bragg peaks positions relating to length q_3 of the scattering vector in the SAXS region. The domain is highlighted by red lines. b – Example of a SAXS diffraction pattern obtained from the domain 3

In Fig. 10a the spatial resolved map of positions of $\{111\}$ and $\{200\}$ reflections are shown simultaneously with red and blue arrows respectively. The domains distinguishable on the spatial-resolved map for the SAXS peaks are highlighted and appear to be the domains for the WAXS peaks. The diffraction patterns in all three domains are characterized by different peak positions shown in Fig. 10b.



a



b

Figure 10. a – spatially resolved map of the Bragg peaks positions relating to Q_{111} (red arrows) and Q_{200} (blue arrows) lengths of the scattering vector in WAXS region. Domains are highlighted by red lines. b – Examples of a WAXS diffraction pattern obtained from the domains 1, 2 and 3. Arrows point on peaks in the WAXS region.

Since these domains contain peaks in both SAXS and WAXS regions, we applied the X-ray Cross-Correlation Analysis to determine the unit cell parameters of these domains and relative orientation of the AL and SL.

3.3. X-ray Cross-Correlation Analysis

Here we calculate the CCF $C(q_1^{SL}, q_{200}^{AL}, \Delta)$ averaged over diffraction patterns in the domains 1 and 2 where there are two pairs of the peaks at q_1^{SL} . The resulting CCFs for both domains are shown in Fig. 11. One can observe four main peaks at $\Delta = \pm 45^\circ$ and $\pm 135^\circ$, representing the relative angles between q_1^{SL} and q_{200}^{AL} . The small peaks at $\Delta = \pm 90^\circ$ could be attributed to the reflections from domains with another orientation, partially illuminated by the considerably big incident beam. Moreover, the peak at $\Delta = -90^\circ$ in the CCF for the domain 2 is absent due to overlapping with the beamstop holder.

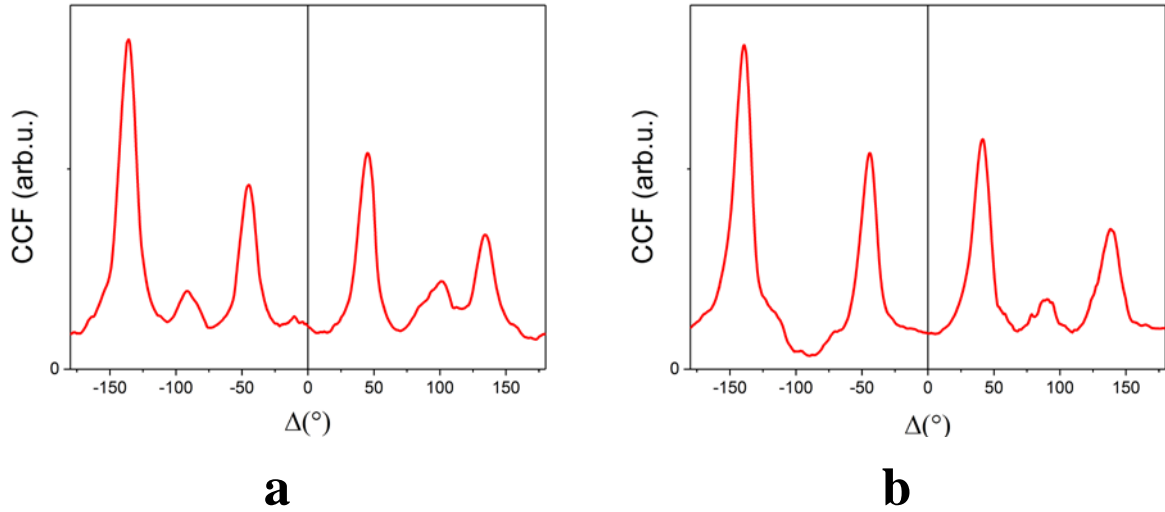


Figure 11. Calculated CCF for q_1 and Q_{200} lengths of scattering vectors: a – for the domain 1 and b – for the domain 2. Black lines represent the symmetry axes.

For the domain 3 containing two pairs of peaks at q_3^{SL} , we calculated the CCF $C(q_3^{SL}, q_{200}^{AL}, \Delta)$ averaged over the whole domain. The obtained CCF is shown in Fig. 12 and contains peaks at $\Delta = -150^\circ, -116^\circ, 31^\circ$ and 65° , representing the relative angles between q_3^{SL} and q_{200}^{AL} . The exact distance between the nearest neighboring peaks is 33.4° .

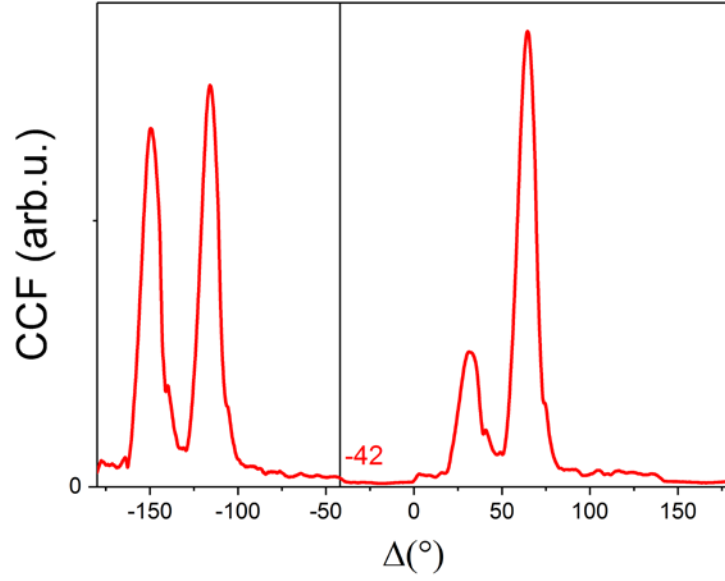


Figure 12. Calculated CCF for q_3 and Q_{200} lengths of scattering vectors in the domain 3. Black lines represent the symmetry axis.

All these angle values could provide us information about unit cell parameters and orientation, but this requires knowledge of which q^{SL} reflexes correspond to which crystalline planes of the SL.

3.4. Superlattice structure evaluation

Bragg peaks could be attributed to the crystalline planes by looking at the radial average of diffraction patterns averaged over all points of the sample. The calculated radial average in the SAXS region is shown in Fig. 13. To resolve non-intense peaks it is given in log scale. It contains several peaks (see Table 1) corresponding to the scattering on the SL of the MC.

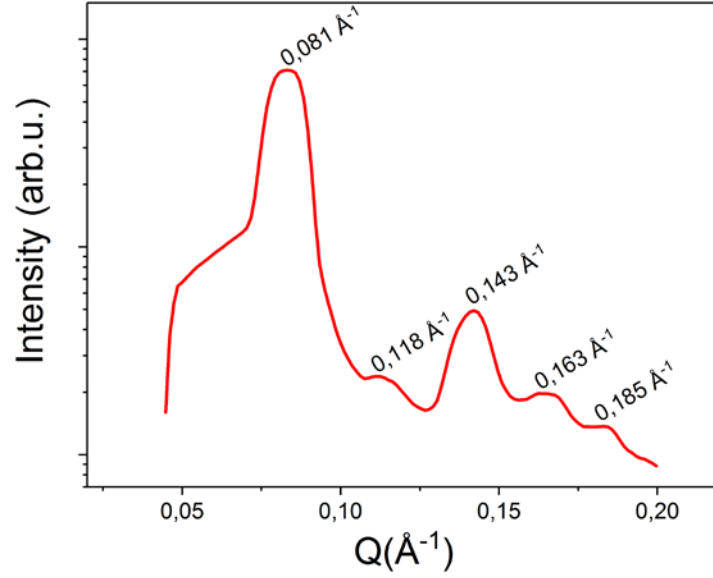


Figure 13. Radial average in log scale in the SAXS region of the diffraction patterns

These values could be fitted by the reflections from a tetragonal unit cell with parameters $a = b = 110 \text{ Å}$ and $c = 142 \text{ Å}$. The indexes of respective reflections are given in Table 1. Since all the $h+k+l$ sums are even, the unit cell could be assumed to have a body-centered tetragonal (bct) structure (shown in Fig. 14) with tetragonal distortion of $\frac{c}{a} = 1.29$.

Table 1. Experimental and simulated parameters of the superlattice unit cell. q_{exp} is the momentum transfer obtained from measurements and q_{predict} is the value of momentum transfer vector calculated from the bct unit cell parameters

$q_{\text{exp}}, \text{Å}^{-1}$		h	k	l		$q_{\text{predict}}, \text{Å}^{-1}$	h+k+l
0,081		1	1	0		0,081	2
0,118		2	0	0		0,114	2
0,143		1	0	3		0,145	4
0,163		2	2	0		0,162	4
0,185		1	2	3		0,184	6

The unit cell of the bct structure is based on three orthogonal vectors \vec{a} , \vec{b} and \vec{c} with moduli $|\vec{a}| = |\vec{b}| = a$ and $|\vec{c}| = c$. Corresponding vectors of the reciprocal lattice are also orthogonal, so the Gram matrix for the reciprocal space is

$$G = 2\pi \begin{pmatrix} \frac{1}{a^2} & 0 & 0 \\ 0 & \frac{1}{a^2} & 0 \\ 0 & 0 & \frac{1}{c^2} \end{pmatrix} \quad (7)$$

The angle 2β between two Bragg peaks from $\{103\}$ reflections can be evaluated as

$$\cos 2\beta = \frac{u^T G v}{\sqrt{u^T G u} \sqrt{v^T G v}} \quad (8)$$

where $u^T = (0 \ 1 \ 3)$ and $v^T = (-1 \ 0 \ 3)$ are the indexes of two reflections. Substituting the Gram matrix (7) and vectors u and v into Eq. (8) and solving the obtained equation for the c/a ratio yields

$$\frac{c}{a} = 3 \sqrt{\frac{1}{\cos^2 2\beta} - 1} \quad (9)$$

Thus, the value of the angle β between $[\bar{1}03]_{\text{SL}}$ and $[013]_{\text{SL}}$ directions for the bct structure of the SL depends on the tetragonal distortion and vice versa. We can evaluate the distortion between a and c dimensions of the unit cell inserting the value $2\beta = 33.4^\circ$ obtained from the XCCA for this domain into Eq. (9), yielding the value of distortion of $\frac{c}{a} = 1.33$, in good agreement with the value obtained from the radial average.

To verify these findings, we modeled a CCF under the assumption of a rock-salt AL and bct SL with $\frac{c}{a} = 1.33$ and the alignment as depicted in Fig. 16.

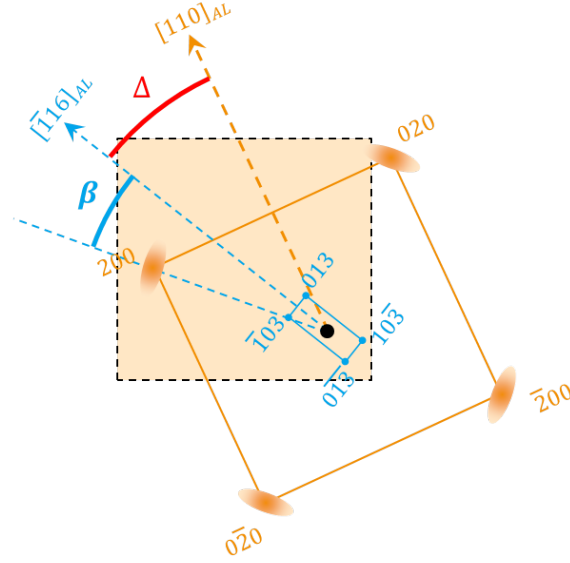


Figure 16. Schematic representation of the AL and the SL in the reciprocal space. Orange ellipsoids represent $\{200\}_{AL}$ reflections from the AL oriented in such a way that the $[001]_{AL}$ direction is perpendicular to the sample surface. Cyan circles represent $\{013\}_{SL}$ reflections from the SL oriented in such a way that the $[441]_{SL}$ direction is perpendicular to the sample surface.

Parameters of the simulation are shown in Table 2. Bragg peaks' positions in the SAXS region are chosen with respect to the angle $\beta = 16.7^\circ$ obtained from the CCF analysis above. The peaks' amplitudes $A_{\frac{SAXS}{WAXS}}$ and angular RMS width $\sigma_{\frac{SAXS}{WAXS}}$ were fitted to the experimentally obtained CCF. The area of reciprocal space covered by the detector is marked in Fig. 16 by a dashed rectangle and respective boundary angles for the mask function are $\varphi_1 = \frac{\pi}{12}$ and $\varphi_2 = \frac{2\pi}{3}$.

Table 2. CCF simulation parameters

$A_{SAXS} = 50$	$A_{WAXS} = 20$
$\varphi_{SAXS} = 0.03 (1.72^\circ)$	$\varphi_{SAXS} = 0.1 (5.72^\circ)$
φ_{SAXS}^i :	φ_{WAXS}^i :
$\pm \text{atan}(0.3),$ $\pi \pm \text{atan}(0.3)$	$\pm \frac{\pi}{4},$ $\pi \pm \frac{\pi}{4}$

The calculated CCF for the experimental data and model CCF for the domain 3 of the sample are shown in Fig. 17. Clearly, they are in a good agreement with each other, which indicates the fidelity of our evaluations of the unit cell distortion. Amplitudes of the peaks in the experimental curve are different because of the varied intensities of the original Bragg peaks in the diffraction patterns.

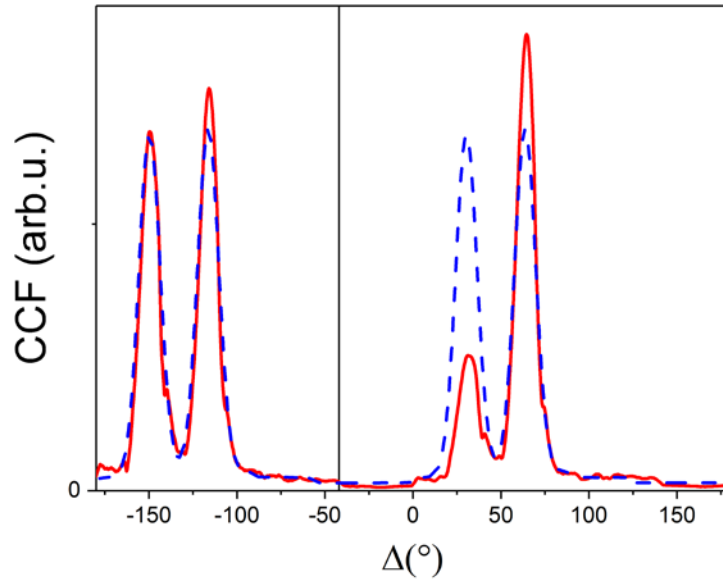


Figure 17. Calculated (red line) CCF for q_3 and Q_{200} lengths of scattering vectors in the domain 3 and model CCF (blue dashed line) obtained assuming that the SL has tetragonal distortion $c/a = 133\%$.

4. Conclusion

In this work we studied diffraction patterns of the MC consisted of PbS NCs and oleic acid linkers. Spatially-resolved maps were obtained for the WAXS and SAXS regions of the collected diffraction patterns. The sample was shown to contain several domains with different orientations of the SL as well as the AL, 3 of them were studied. The unit cell structure of the SL was evaluated by the analysis of the diffraction patterns in the SAXS region. The MC was shown to have the body-centered tetragonal lattice with tetragonal distortion $\frac{c}{a} = 1.29$. By the XCCA analysis, this structure was confirmed. CCF calculated for the domains 1 and 2 were attributed to the $\{110\}$ reflections and indicated absence of the distortion between the a and b dimensions of the unit cell. Whereas the CCF for the domain 3 contained information about distortion between the a and c dimensions and the distortion value was specified to be $\frac{c}{a} = 1.33$. The cross-correlation function for the bct lattice with

obtained value of distortion was modeled and was in good agreement with the experimental CCF, confirming the obtained crystalline structure.

References

1. Song, Rui-Qi, and Helmut Cölfen. "Mesocrystals—ordered nanoparticle superstructures." *Advanced materials* 22.12 (2010): 1301-1330.
2. André, Alexander, et al. "Toward conductive mesocrystalline assemblies: PbS nanocrystals cross-linked with tetrathiafulvalene dicarboxylate." *Chemistry of Materials* 27.23 (2015): 8105-8115.
3. Boneschanscher, Mark P., et al. "Long-range orientation and atomic attachment of nanocrystals in 2D honeycomb superlattices." *Science* 344.6190 (2014): 1377-1380.
4. Salditt, Tim, et al. "Partially coherent nano-focused x-ray radiation characterized by Talbot interferometry." *Optics express* 19.10 (2011): 9656-9675.
5. Kurta, Ruslan, et al. "Structural Analysis by X-ray Intensity Angular Cross Correlations." In *Advances in Chemical Physics*, Volume 161; John Wiley & Sons, Inc. (2016): 1-39.
6. Zaluzhnyy, Ivan, et al. "Quantifying Angular Correlations between the Atomic Lattice and Superlattice of Nanocrystals Assembled with Directional Linking." *Nano Letters* (2017).
7. Gurin, V. S. "Nucleation and growth of PbS nanocrystals and simulation of X-ray diffraction patterns." *Journal of crystal growth* 191.1 (1998): 161-165.